Available online at www.sciencedirect.com

SCIENCE DIRECT®

Journal of Computational Physics 193 (2003) 115–135

JOURNAL OF COMPUTATIONAL PHYSICS

www.elsevier.com/locate/jcp

Hermite WENO schemes and their application as limiters for Runge–Kutta discontinuous Galerkin method: one-dimensional case

Jianxian Qiu [a,1], Chi-Wang Shu [b,*,2]

[a] *Department of Mathematics, University of Science and Technology of China, Hefei, Anhui 230026, PR China*
[b] *Division of Applied Mathematics, Brown University, Providence, RI 02912, USA*

Received 16 May 2003; received in revised form 23 July 2003; accepted 23 July 2003

Abstract

In this paper, a class of fifth-order weighted essentially non-oscillatory (WENO) schemes based on Hermite polynomials, termed HWENO (Hermite WENO) schemes, for solving one-dimensional nonlinear hyperbolic conservation law systems is presented. The construction of HWENO schemes is based on a finite volume formulation, Hermite interpolation, and nonlinearly stable Runge–Kutta methods. The idea of the reconstruction in the HWENO schemes comes from the original WENO schemes, however both the function and its first derivative values are evolved in time and used in the reconstruction, while only the function values are evolved and used in the original WENO schemes. Comparing with the original WENO schemes of Liu et al. [J. Comput. Phys. 115 (1994) 200] and Jiang and Shu [J. Comput. Phys. 126 (1996) 202], one major advantage of HWENO schemes is its compactness in the reconstruction. For example, five points are needed in the stencil for a fifth-order WENO (WENO5) reconstruction, while only three points are needed for a fifth-order HWENO (HWENO5) reconstruction. For this reason, the HWENO finite volume methodology is more suitable to serve as limiters for the Runge–Kutta discontinuous Galerkin (RKDG) methods, than the original WENO finite volume methodology. Such applications in one space dimension is also developed in this paper.

AMS: 65M06; 65M60; 65M99; 35L65

Keywords: WENO scheme; Hermite interpolation; High order accuracy; Runge–Kutta discontinuous Galerkin method; Limiters

* Corresponding author. Tel.: +401-863-2549; fax: +401-863-1355.
E-mail addresses: jxqiu@ustc.edu.cn (J. Qiu), shu@dam.brown.edu (C.-W. Shu).

[1] The research of this author is supported by NNSFC grant 10028103.

[2] The research of this author is supported by NNSFC grant 10028103 while he is in residence at the Department of Mathematics, University of Science and Technology of China, Hefei, Anhui 230026, PR China. Additional support is provided by ARO grant DAAD19-00-1-0405 and NSF grant DMS-0207451.

0021-9991/$ - see front matter
doi:10.1016/j.jcp.2003.07.026

1. Introduction

In this paper, we first construct a class of fifth-order weighted essentially non-oscillatory (WENO) schemes based on Hermite polynomials, termed HWENO (Hermite WENO) schemes, for solving one-dimensional (1D) nonlinear hyperbolic conservation law systems

$$\begin{cases} u_t + f(u)_x = 0, \\ u(x,0) = u_0(x). \end{cases} \tag{1.1}$$

We then apply this HWENO finite volume methodology as limiters for the Runge–Kutta discontinuous Galerkin (RKDG) methods. Only 1D case is considered in this paper. While the methodology can be generalized in principle to multi dimensions, more work is needed to carry out the detailed design and this is left for future research.

WENO schemes have been designed in recent years as a class of high order finite volume or finite difference schemes to solve hyperbolic conservation laws with the property of maintaining both uniform high order accuracy and an essentially non-oscillatory shock transition. The first WENO scheme is constructed in [19] for a third-order finite volume version in one space dimension. In [17], third and fifth-order finite difference WENO schemes in multi space dimensions are constructed, with a general framework for the design of the smoothness indicators and nonlinear weights. Finite difference WENO schemes of higher orders (seventh to 11th order) are constructed in [1], and finite volume versions on unstructured and structured meshes are designed in, e.g. [13,16,18,21,24]. WENO schemes are designed based on the successful ENO schemes in [15,27,28]. Both ENO and WENO schemes use the idea of adaptive stencils in the reconstruction procedure based on the local smoothness of the numerical solution to automatically achieve high order accuracy and a non-oscillatory property near discontinuities. ENO uses just one (optimal in some sense) out of many candidate stencils when doing the reconstruction; while WENO uses a convex combination of all the candidate stencils, each being assigned a nonlinear weight which depends on the local smoothness of the numerical solution based on that stencil. WENO improves upon ENO in robustness, better smoothness of fluxes, better steady state convergence, better provable convergence properties, and more efficiency. For a detailed review of ENO and WENO schemes, we refer to the lecture notes [26].

The framework of the finite volume and finite difference WENO schemes is to evolve only one degree of freedom per cell, namely the cell average for the finite volume version or the point value at the center of the cell for the finite difference version. High order accuracy is achieved through a WENO reconstruction which uses a stencil of k cells for kth order accuracy. Thus a fifth-order WENO scheme would need the information from five neighboring cells in order to reconstruct the numerical flux. There are efforts in the literature to design schemes using a narrower stencil to achieve the same order of accuracy, through the evolution of more than one degree of freedom per cell. For example, non-negativity, monotonicity or convexity preserving cubic and quintic Hermite interpolation is discussed in [12]; various CIP type schemes based on Hermite type interpolations are developed in, e.g. [20,29], and a second-order TVD scheme satisfying all entropy conditions, based on evolving both the cell average and the slope per cell, is designed in [3]. In the first part of this paper we follow this line of research and construct a class of fifth-order WENO schemes based on Hermite polynomials, termed HWENO (Hermite WENO) schemes, for solving the 1D nonlinear hyperbolic conservation law systems (1.1). The construction of HWENO schemes is based on a finite volume formulation, Hermite interpolation, and nonlinearly stable Runge–Kutta methods. The idea of the reconstruction in the HWENO schemes comes from the original WENO schemes, however both the function and its first derivative values are evolved in time and used in the reconstruction, while only the function values are evolved and used in the original WENO schemes. Comparing with the original WENO schemes of Liu et al. [19] and Jiang and Shu [17], one major advantage of HWENO schemes is its

compactness in the reconstruction. For example, five points are needed in the stencil for a fifth-order WENO (WENO5) reconstruction, while only three points are needed for a fifth-order HWENO (HWENO5) reconstruction.

The discontinuous Galerkin (DG) method can be considered as an extreme in the methodology described above. It evolves k degrees of freedom (in one dimension) per cell for a kth order accurate scheme, thus no reconstruction is needed. The first DG method was introduced in 1973 by Reed and Hill [23], in the framework of neutron transport (steady state linear hyperbolic equations). A major development of the DG method was carried out by Cockburn et al. in a series of papers [5–9], in which they established a framework to easily solve *nonlinear* time dependent hyperbolic conservation laws (1.1) using explicit, nonlinearly stable high order Runge–Kutta time discretizations [27] and DG discretization in space with exact or approximate Riemann solvers as interface fluxes and TVB (total variation bounded) limiter [25] to achieve non-oscillatory properties for strong shocks. These schemes are termed Runge–Kutta discontinuous Galerkin (RKDG) methods. For a review of RKDG methods, see [10].

An important component of RKDG methods for solving conservation laws (1.1) with strong shocks in the solutions is a nonlinear limiter, which is applied to control spurious oscillations. Although many limiters exist in the literature, e.g. [2,4–9], they tend to degenerate accuracy when mistakenly used in smooth regions of the solution. In [22], we initialized a study of using WENO methodology as limiters for RKDG methods. The idea is to first identify "troubled cells", namely those cells where limiting might be needed, then to abandon all moments in those cells except the cell averages and reconstruct those moments from the information of neighboring cells using a WENO methodology. This technique works quite well in our one and two-dimensional (2D) test problems [22]. However, one place in the approach of [22] which would welcome improvements is that the reconstruction for the moments in troubled cells has to use the cell average information from $2k+1$ neighboring cells, for $(k+1)$th order RKDG methods of piecewise polynomials of degree k. This stencil is significantly wider than the original RKDG methodology. For this reason, the HWENO finite volume method developed in this paper is more suitable to serve as limiters for the RKDG methods, since it uses much fewer neighboring cells to obtain a reconstruction of the same order of accuracy. Such applications in one space dimension is also developed in this paper.

The organization of this paper is as follows. In Section 2, we describe in detail the construction and implementation of HWENO schemes with Runge–Kutta time discretizations, for 1D scalar and system equations (1.1). In Section 3, we investigate the usage of the HWENO finite volume methodology as limiters for RKDG methods, following the idea in [22], with the goal of obtaining a robust and high order limiting procedure to simultaneously obtain uniform high order accuracy and sharp, non-oscillatory shock transition for RKDG methods. In Section 4 we provide extensive numerical examples to demonstrate the behavior of the HWENO schemes and DG methods with HWENO limiters with Runge–Kutta time discretizations. Concluding remarks are given in Section 5.

2. The construction of Hermite WENO schemes

In this section we first consider 1D scalar conservation laws (1.1). For simplicity, we assume that the grid points $\{x_i\}$ are uniformly distributed with the cell size $x_{i+1}-x_i=\Delta x$ and cell centers $x_{i+1/2}=\frac{1}{2}(x_i+x_{i+1})$. We also denote the cells by $I_i=[x_{i-1/2},x_{i+1/2}]$.

Let $v=u_x$ and $g(u,v)=f'(u)u_x=f'(u)v$. From (1.1) and its spatial derivative we obtain

$$\begin{cases} u_t+f(u)_x=0, & u(x,0)=u_0(x),\\ v_t+g(u,v)_x=0, & v(x,0)=v_0(x). \end{cases} \tag{2.1}$$

We denote the cell averages of u and v as

$$\overline{u}_i(t) = \frac{1}{\Delta x}\int_{I_i} u(x,t)\,\mathrm{d}x, \quad \overline{v}_i(t) = \frac{1}{\Delta x}\int_{I_i} v(x,t)\,\mathrm{d}x.$$

Integrating (2.1) over the cell I_i we obtain an equivalent formulation of the conservation laws

$$\begin{cases} \frac{\mathrm{d}\overline{u}_i(t)}{\mathrm{d}t} = -\frac{1}{\Delta x}(f(u(x_{i+1/2},t)) - f(u(x_{i-1/2},t))), \\ \frac{\mathrm{d}\overline{v}_i(t)}{\mathrm{d}t} = -\frac{1}{\Delta x}(g(u(x_{i+1/2},t),v(x_{i+1/2},t)) - g(u(x_{i-1/2},t),v(x_{i-1/2},t))). \end{cases} \tag{2.2}$$

We approximate (2.2) by the following conservative scheme

$$\begin{cases} \frac{\mathrm{d}\overline{u}_i(t)}{\mathrm{d}t} = -\frac{1}{\Delta x}(\hat{f}_{i+1/2} - \hat{f}_{i-1/2}), \\ \frac{\mathrm{d}\overline{v}_i(t)}{\mathrm{d}t} = -\frac{1}{\Delta x}(\hat{g}_{i+1/2} - \hat{g}_{i-1/2}), \end{cases} \tag{2.3}$$

where the numerical fluxes $\hat{f}_{i+1/2}$ and $\hat{g}_{i+1/2}$ are defined by:

$$\begin{aligned} \hat{f}_{i+1/2} &= h\left(u^-_{i+1/2}, u^+_{i+1/2}\right), \\ \hat{g}_{i+1/2} &= H\left(u^-_{i+1/2}, u^+_{i+1/2}; v^-_{i+1/2}, v^+_{i+1/2}\right), \end{aligned} \tag{2.4}$$

where $u^\pm_{i+1/2}$ and $v^\pm_{i+1/2}$ are numerical approximations to the point values of $u(x_{i+1/2},t)$ and $v(x_{i+1/2},t)$ respectively from left and right. The fluxes in (2.4) are subject to the usual conditions for numerical fluxes, such as Lipschitz continuity and consistency with the physical fluxes $f(u)$ and $g(u,v)$.

In this paper we use the following local Lax–Friedrichs fluxes:

$$\begin{aligned} h(a,b) &= \frac{1}{2}[f(a) + f(b) - \alpha(b-a)], \\ H(a,b;c,d) &= \frac{1}{2}[g(a,c) + g(b,d) - \alpha(d-c)], \end{aligned} \tag{2.5}$$

where $\alpha = \max_{u\in D}|f'(u)|$, with $D = [\min(a,b), \max(a,b)]$.

The method of lines ODE (2.3) is then discretized in time by a TVD Runge–Kutta method in [27]. The third-order version in [27] is used in this paper.

The first-order "building block" of this scheme can be obtained by using the cell averages $\overline{u}_i$ and $\overline{v}_i$ to replace the point values $u^-_{i+1/2}$, $u^+_{i-1/2}$ and $v^-_{i+1/2}$, $v^+_{i-1/2}$ respectively, and using Euler forward for the time discretization. The result is the following scheme

$$\begin{cases} \overline{u}_i^{n+1} = \overline{u}_i^n - \lambda\left(h(\overline{u}_i^n, \overline{u}_{i+1}^n) - h(\overline{u}_{i-1}^n, \overline{u}_i^n)\right), \\ \overline{v}_i^{n+1} = \overline{v}_i^n - \lambda\left(H(\overline{u}_i^n, \overline{u}_{i+1}^n; \overline{v}_i^n, \overline{v}_{i+1}^n) - H(\overline{u}_{i-1}^n, \overline{u}_i^n; \overline{v}_{i-1}^n, \overline{v}_i^n)\right) \end{cases} \tag{2.6}$$

with the numerical fluxes h and H defined by (2.5). Here $\lambda = \Delta t/\Delta x$. For this building block we have the following total variation stability result, where for simplicity we assume α is a constant:

Proposition 2.1. *The scheme* (2.6)*, with the numerical fluxes h and H defined by* (2.5) *and under the CFL condition* $\lambda\alpha \leqslant 1$*, satisfies*

$$TV(\overline{u}^{n+1}) \leqslant TV(\overline{u}^n), \quad ||\overline{v}^{n+1}||_{L^1} \leqslant ||\overline{v}^n||_{L^1},$$

where the norms are defined by

$$TV(\overline{u}) \equiv \sum_i |\overline{u}_{i+1} - \overline{u}_i|, \quad ||\overline{v}||_{L^1} \equiv \sum_i |\overline{v}_i|\Delta x.$$

Proof. The total variation diminishing property $TV(\overline{u}^{n+1}) \leqslant TV(\overline{u}^n)$ is a consequence of the monotone scheme satisfied by $\overline{u}$, see for example [11]. We thus prove only the L^1 stability result for $\overline{v}$. By using definitions of the scheme (2.6) and the numerical fluxes (2.5) we obtain

$$\begin{aligned}
\frac{1}{\Delta x}||\overline{v}^{n+1}||_{L^1} &= \sum_i \left| \overline{u}_i^n - \frac{\lambda}{2}\left(f'\left(\overline{u}_{i+1}^n\right)\overline{v}_{i+1}^n - f'\left(\overline{u}_{i-1}^n\right)\overline{v}_{i-1}^n - \alpha\left(\overline{v}_{i+1}^n - 2\overline{v}_i^n + \overline{v}_{i-1}^n\right)\right)\right| \\
&= \sum_i \left| (1-\lambda\alpha)\overline{v}_i^n + \frac{\lambda}{2}\left(\alpha - f'\left(\overline{u}_{i+1}^n\right)\right)\overline{v}_{i+1}^n + \frac{\lambda}{2}\left(\alpha + f'\left(\overline{u}_{i-1}^n\right)\right)\overline{v}_{i-1}^n \right| \\
&\leqslant \sum_i (1-\lambda\alpha)\left|\overline{v}_i^n\right| + \sum_i \frac{\lambda}{2}\left(\alpha - f'\left(\overline{u}_i^n\right)\right)\left|\overline{v}_i^n\right| + \sum_i \frac{\lambda}{2}\left(\alpha + f'\left(\overline{u}_i^n\right)\right)\left|\overline{v}_i^n\right| \\
&= \sum_i \left|\overline{v}_i^n\right| = \frac{1}{\Delta x}||\overline{v}^n||_{L^1}.
\end{aligned}$$

Here, we have used the definition of α and the CFL condition $\lambda\alpha \leqslant 1$ in the inequality above and have ignored boundary terms by assuming periodic or compact boundary conditions. □

Since v approximates the derivative of u, the L^1 norm of $\overline{v}$ is equivalent to the total variation norm of u. Thus the proposition indicates that the base first-order scheme is TVD, both in a direct measurement of the total variation norm of $\overline{u}$ and in an indirect measurement of the total variation norm of u through the L^1 norm of $\overline{v}$. This gives us a solid foundation to build higher order schemes using this building block.

The key component of the HWENO schemes is the reconstruction, from the cell averages $\{\overline{u}_i, \overline{v}_i\}$ to the points values $\{u_{i+1/2}^{\pm}, v_{i+1/2}^{\pm}\}$. This reconstruction should be both high order accurate and essentially non-oscillatory. We outline the procedure of this reconstruction for the fifth-order accuracy case in the following.

Step 1. Reconstruction of $\{u_{i+1/2}^{\pm}\}$ by HWENO from the cell averages $\{\overline{u}_i, \overline{v}_i\}$.

1. Given the small stencils $S_0 = \{I_{i-1}, I_i\}$, $S_1 = \{I_i, I_{i+1}\}$ and the bigger stencil $\mathscr{T} = \{S_0, S_1\}$, we construct Hermite quadratic reconstruction polynomials $p_0(x), p_1(x), p_2(x)$ and a fourth-degree reconstruction polynomial $q(x)$ such that:

$$\frac{1}{\Delta x}\int_{I_{i+j}} p_0(x)\,\mathrm{d}x = \overline{u}_{i+j}, \quad j = -1, 0, \quad \frac{1}{\Delta x}\int_{I_{i-1}} p_0'(x)\,\mathrm{d}x = \overline{v}_{i-1},$$

$$\frac{1}{\Delta x}\int_{I_{i+j}} p_1(x)\,\mathrm{d}x = \overline{u}_{i+j}, \quad j = 0, 1, \quad \frac{1}{\Delta x}\int_{I_{i+1}} p_1'(x)\,\mathrm{d}x = \overline{v}_{i+1},$$

$$\frac{1}{\Delta x}\int_{I_{i+j}} p_2(x)\,\mathrm{d}x = \overline{u}_{i+j}, \quad j = -1, 0, 1.$$

$$\frac{1}{\Delta x}\int_{I_{i+j}} q(x)\,\mathrm{d}x = \overline{u}_{i+j}, \quad j = -1, 0, 1, \quad \frac{1}{\Delta x}\int_{I_{i+j}} q'(x)\,\mathrm{d}x = \overline{v}_{i+j}, \quad j = -1, 1.$$

In fact, we only need the values of these polynomials at the cell boundary $x_{i+1/2}$ given in terms of the cell averages, which have the following expressions:

$$p_0(x_{i+1/2}) = -\frac{7}{6}\overline{u}_{i-1} + \frac{13}{6}\overline{u}_i - \frac{2\Delta x}{3}\overline{v}_{i-1},$$

$$p_1(x_{i+1/2}) = \frac{1}{6}\overline{u}_i + \frac{5}{6}\overline{u}_{i+1} - \frac{\Delta x}{3}\overline{v}_{i+1},$$

$$p_2(x_{i+1/2}) = -\frac{1}{6}\overline{u}_{i-1} + \frac{5}{6}\overline{u}_i + \frac{1}{3}\overline{u}_{i+1},$$

$$q(x_{i+1/2}) = -\frac{23}{120}\overline{u}_{i-1} + \frac{19}{30}\overline{u}_i + \frac{67}{120}\overline{u}_{i+1} - \Delta x\left(\frac{3}{40}\overline{v}_{i-1} + \frac{7}{40}\overline{v}_{i+1}\right).$$

2. We find the combination coefficients, also called linear weights, denoted by γ_0, γ_1 and γ_2, satisfying:

$$q(x_{i+1/2}) = \sum_{j=0}^{2} \gamma_j p_j(x_{i+1/2})$$

for all the cell averages of u and v in the bigger stencil $\mathscr{T}$. This leads to

$$\gamma_0 = \frac{9}{80}, \quad \gamma_1 = \frac{21}{40}, \quad \gamma_2 = \frac{29}{80}.$$

3. We compute the smoothness indicator, denoted by β_j, for each stencil S_j, which measures how smooth the function $p_j(x)$ is in the target cell I_i. The smaller this smoothness indicator β_j, the smoother the function $p_j(x)$ is in the target cell. We use the same recipe for the smoothness indicator as in [17]

$$\beta_j = \sum_{l=1}^{2} \int_{I_i} \Delta x^{2l-1} \left(\frac{\partial^l}{\partial x^l} p_j(x)\right)^2 \mathrm{d}x. \tag{2.7}$$

In the actual numerical implementation the smoothness indicators β_j are written out explicitly as quadratic forms of the cell averages of u and v in the stencil:

$$\beta_0 = (-2\overline{u}_{i-1} + 2\overline{u}_i - \Delta x\overline{v}_{i-1})^2 + \frac{13}{3}(-\overline{u}_{i-1} + \overline{u}_i - \Delta x\overline{v}_{i-1})^2,$$

$$\beta_1 = (-2\overline{u}_i + 2\overline{u}_{i+1} - \Delta x\overline{v}_{i+1})^2 + \frac{13}{3}(-\overline{u}_i + \overline{u}_{i+1} + \Delta x\overline{v}_{i+1})^2,$$

$$\beta_2 = \frac{1}{4}(-\overline{u}_{i-1} + \overline{u}_{i+1})^2 + \frac{13}{12}(-\overline{u}_{i-1} + 2\overline{u}_i - \overline{u}_{i+1})^2.$$

4. We compute the nonlinear weights based on the smoothness indicators

$$\omega_j = \frac{\overline{\omega}_j}{\sum_k \overline{\omega}_k}, \quad \overline{\omega}_k = \frac{\gamma_k}{(\varepsilon + \beta_k)^2}, \tag{2.8}$$

where γ_k are the linear weights determined in Step 1.2 above, and ε is a small number to avoid the denominator to become 0. We are using $\varepsilon = 10^{-6}$ in all the computation in this paper. The final HWENO reconstruction is then given by

$$u^-_{i+1/2} \approx \sum_{j=0}^{2} \omega_j p_j(x_{i+1/2}). \tag{2.9}$$

The reconstruction to $u^+_{i-1/2}$ is mirror symmetric with respect to x_i of the above procedure.

Step 2. Reconstruction of the derivative values $\{v^{\pm}_{i+1/2}\}$ by HWENO from the cell averages $\{\overline{u}_i, \overline{v}_i\}$.

5. Given the small stencils $S_0 = \{I_{i-1}, I_i\}$, $S_1 = \{I_i, I_{i+1}\}$ and the bigger stencil $\mathscr{T} = \{S_0, S_1\}$, we construct Hermite cubic reconstruction polynomials $p_0(x), p_1(x), p_2(x)$ and a fifth-degree reconstruction polynomial $q(x)$ such that:

$$\frac{1}{\Delta x}\int_{I_{i+j}} p_0(x)\,\mathrm{d}x = \overline{u}_{i+j}, \quad \frac{1}{\Delta x}\int_{I_{i+j}} p_0'(x)\,\mathrm{d}x = \overline{v}_{i+j}, \quad j = -1, 0,$$

$$\frac{1}{\Delta x}\int_{I_{i+j}} p_1(x)\,\mathrm{d}x = \overline{u}_{i+j}, \quad \frac{1}{\Delta x}\int_{I_{i+j}} p_1'(x)\,\mathrm{d}x = \overline{v}_{i+j}, \quad j = 0, 1,$$

$$\frac{1}{\Delta x}\int_{I_{i+j}} p_2(x)\,\mathrm{d}x = \overline{u}_{i+j}, \quad j = -1, 0, 1, \quad \frac{1}{\Delta x}\int_{I_i} p_2'(x)\,\mathrm{d}x = \overline{v}_i,$$

$$\frac{1}{\Delta x}\int_{I_{i+j}} q(x)\,\mathrm{d}x = \overline{u}_{i+j}, \quad \frac{1}{\Delta x}\int_{I_{i+j}} q'(x)\,\mathrm{d}x = \overline{v}_{i+j}, \quad j = -1, 0, 1.$$

In fact, we only need the values of the derivative of these polynomials at the cell boundary $x_{i+1/2}$ given in terms of the cell averages, which have the following expressions:

$$p_0'(x_{i+1/2}) = \frac{4}{\Delta x}(\overline{u}_{i-1} - \overline{u}_i) + \frac{3}{2}\overline{v}_{i-1} + \frac{7}{2}\overline{v}_i,$$

$$p_1'(x_{i+1/2}) = \frac{2}{\Delta x}(-\overline{u}_{i-1} + \overline{u}_i) - \frac{1}{2}\overline{v}_i - \frac{1}{2}\overline{v}_{i+1},$$

$$p_2'(x_{i+1/2}) = \frac{1}{4\Delta x}(\overline{u}_{i-1} - 4\overline{u}_i + 3\overline{u}_{i+1}) + \frac{1}{2}\overline{v}_i,$$

$$q'(x_{i+1/2}) = \frac{1}{\Delta x}\left(\frac{1}{4}\overline{u}_{i-1} - 2\overline{u}_i + \frac{7}{4}\overline{u}_{i+1}\right) + \frac{1}{12}\overline{v}_{i-1} - \frac{1}{6}\overline{v}_i - \frac{5}{12}\overline{v}_{i+1}.$$

6. Compute linear weights γ_0', γ_1' and γ_2', satisfying

$$q'(x_{i+1/2}) = \sum_{j=0}^{2} \gamma_j' p_j'(x_{i+1/2})$$

for all the cell averages of u and v in the bigger stencil $\mathscr{T}$. This leads to

$$\gamma_0' = \frac{1}{18}, \quad \gamma_1' = \frac{5}{6}, \quad \gamma_2' = \frac{1}{9}.$$

7. We define the smoothness indicators for the reconstruction of derivatives as

$$\beta_j = \sum_{l=2}^{3} \int_{I_i} (\Delta x)^{(2l-1)} \left(\frac{\partial^l}{\partial x^l} p_j(x)\right)^2 \mathrm{d}x. \tag{2.10}$$

Notice that the summation starts from the second derivative rather than from the first, as we are now reconstructing the first derivative rather than the function values. We can again write these smoothness indicators out explicitly as quadratic forms of the cell averages of u and v in the stencil:

$$\beta_0 = 4(3(\overline{u}_{i-1} - \overline{u}_i) + \Delta x(\overline{v}_{i-1} + 2\overline{v}_i))^2 + \frac{39}{4}(2(\overline{u}_{i-1} - \overline{u}_i) + \Delta x(\overline{v}_{i-1} + \overline{v}_i))^2,$$

$$\beta_1 = 4(-3(\overline{u}_i - \overline{u}_{i+1}) - \Delta x(2\overline{v}_i + \overline{v}_{i+1}))^2 + \frac{39}{4}(2(\overline{u}_i - \overline{u}_{i+1}) + \Delta x(\overline{v}_i + \overline{v}_{i+1}))^2,$$

$$\beta_2 = (\overline{u}_{i-1} - 2\overline{u}_i + \overline{u}_{i+1})^2 + \frac{39}{16}(\overline{u}_{i+1} - \overline{u}_{i-1} - 2\Delta x\overline{v}_i)^2.$$

8. We compute the nonlinear weights by

$$\omega_j = \frac{\overline{\omega}_j}{\sum_k \overline{\omega}_k}, \quad \overline{\omega}_k = \frac{\gamma'_k}{(\varepsilon + \beta_k)^2}. \tag{2.11}$$

The final HWENO reconstruction to $v^-_{i+1/2}$ is then given by

$$v^-_{i+1/2} \approx \sum_{j=0}^{2} \omega_j p'_j(x_{i+1/2}). \tag{2.12}$$

The reconstruction to $v^+_{i-1/2}$ is mirror symmetric with respect to x_i of the above procedure. □

We remark that a more natural procedure would have been using the same small stencils and lower order polynomials in both Step 1 and Step 2 above, which would have saved computational time as the costly smoothness indicators would have to be computed only once. Unfortunately this does not work as suitable linear weights do not exist in Step 2.2 above for such choices.

For systems of conservation laws, such as the Euler equations of gas dynamics, both of the reconstructions from $\{\overline{u}_i, \overline{v}_i\}$ to $\{u^\pm_{i+1/2}\}$ and $\{v^\pm_{i+1/2}\}$ are performed in the local characteristic directions to avoid oscillation. For details of such local characteristic decompositions, see, e.g. [26].

3. HWENO reconstruction as limiters for the discontinuous Galerkin method

In [22], we have started the study of using WENO reconstruction methodology as limiters for the RKDG methods. The first step in the procedure is to identify the "troubled cells", namely those cells which might need the limiting procedure. In [22] as well as in this paper, we use the usual minmod type TVB limiters as in [5,7,9]. That is, whenever the minmod limiter changes the slope, the cell is declared to be a troubled cell. This identification of troubled cells is not optimal. Often smooth cells, especially those near smooth extrema, are mistakenly identified as troubled cells. However, the idea of using WENO reconstructions in those cells is to maintain high order accuracy even if smooth cells are mistaken as troubled cells. The second step is to replace the solution polynomials in the troubled cells by reconstructed polynomials which maintain the original cell averages (for conservation), have the same order of accuracy as before, but are less oscillatory. In [22], regular finite volume type WENO reconstruction based on cell averages of neighbors is used for the second step. In this section, we apply the HWENO reconstruction procedure developed in the previous section for the second step, which reduces the stencil of the reconstruction while maintaining the same high order accuracy.

The DG solution as well as the test function space is given by $V_h^k = \{p : p|_{I_i} \in P^k(I_i)\}$, where $P^k(I_i)$ is the space of polynomials of degree $\leqslant k$ on the cell I_i. We adopt a local orthogonal basis over I_i, $\{v_l^{(i)}(x), l = 0, 1, \ldots, k\}$, namely the scaled Legendre polynomials

$$v_0^{(i)}(x) = 1, \quad v_1^{(i)}(x) = \frac{x - x_i}{\Delta x_i}, \quad v_2^{(i)}(x) = \left(\frac{x - x_i}{\Delta x_i}\right)^2 - \frac{1}{12}, \ldots$$

Then the numerical solution $u^h(x,t)$ in the space V_h^k can be written as

$$u^h(x,t) = \sum_{l=0}^{k} u_i^{(l)}(t) v_l^{(i)}(x) \quad \text{for } x \in I_i \tag{3.1}$$

and the degrees of freedom $u_i^{(l)}(t)$ are the moments defined by

$$u_i^{(l)}(t) = \frac{1}{a_l} \int_{I_i} u^h(x,t) v_l^{(i)}(x)\,\mathrm{d}x, \quad l = 0, 1, \ldots, k,$$

where $a_l = \int_{I_i} (v_l^{(i)}(x))^2\,\mathrm{d}x$ are the normalization constants since the basis is not orthonormal. In order to determine the approximate solution, we evolve the degrees of freedom $u_i^{(l)}$

$$\begin{aligned} &\frac{\mathrm{d}}{\mathrm{d}t} u_i^{(l)} + \frac{1}{a_l}\left(- \int_{I_i} f(u^h(x,t)) \frac{\mathrm{d}}{\mathrm{d}x} v_l^{(i)}(x)\,\mathrm{d}x + \hat{f}\left(u_{i+1/2}^-, u_{i+1/2}^+\right) v_l^{(i)}(x_{i+1/2}) \right. \\ &\quad \left. - \hat{f}\left(u_{i-1/2}^-, u_{i+1/2}^-\right) v_l^{(i)}(x_{i-1/2}) \right) = 0, \quad l = 0, 1, \ldots, k, \end{aligned} \tag{3.2}$$

where $u_{i+1/2}^{\pm} = u^h(x_{i+1/2}^{\pm}, t)$ are the left and right limits of the discontinuous solution u^h at the cell interface $x_{i+1/2}$, $\hat{f}(u^-, u^+)$ is a monotone flux (non-decreasing in the first argument and non-increasing in the second argument) for the scalar case and an exact or approximate Riemann solver for the system case. The semidiscrete scheme (3.2) is discretized in time by a nonlinearly stable Runge–Kutta time discretization, e.g. the third-order version in [27]. The integral term in (3.2) can be computed either exactly or by a suitable numerical quadrature accurate to at least $O(\Delta x^{k+l+2})$.

The limiter adopted in [7] is described below in some detail, as it is the one used in [22] and in this paper to detect "troubled cells". Denote

$$u_{i+1/2}^- = u_i^{(0)} + \tilde{\boldsymbol{u}}_i, \quad u_{i-1/2}^+ = u_i^{(0)} - \tilde{\tilde{\boldsymbol{u}}}_i$$

From (3.1) we can see that

$$\tilde{\boldsymbol{u}}_i = \sum_{l=1}^{k} u_i^{(l)} v_l^{(i)}(x_{i+1/2}), \quad \tilde{\tilde{\boldsymbol{u}}}_i = -\sum_{l=1}^{k} u_i^{(l)} v_l^{(i)}(x_{i-1/2}).$$

These are modified by either the standard minmod limiter [14]

$$\tilde{\boldsymbol{u}}_i^{(\mathrm{mod})} = m\left(\tilde{\boldsymbol{u}}_i, \Delta_+ u_i^{(0)}, \Delta_- u_i^{(0)}\right), \quad \tilde{\tilde{\boldsymbol{u}}}_i^{(\mathrm{mod})} = m(\tilde{\tilde{\boldsymbol{u}}}_i, \Delta_+ u_i^{(0)}, \Delta_- u_i^{(0)}),$$

where m is given by

$$m(a_1, a_2, \ldots, a_n) = \begin{cases} s \cdot \min_{1 \leqslant j \leqslant n} |a_j| & \text{if } \operatorname{sign}(a_1) = \operatorname{sign}(a_2) = \cdots = \operatorname{sign}(a_n) = s, \\ 0 & \text{otherwise} \end{cases} \tag{3.3}$$

or by the TVB modified minmod function [25]

$$\tilde{m}(a_1, a_2, \ldots, a_n) = \begin{cases} a_1 & \text{if } |a_1| \leqslant M\Delta x^2, \\ m(a_1, a_2, \ldots, a_n) & \text{otherwise,} \end{cases} \tag{3.4}$$

where $M > 0$ is a constant. The choice of M depends on the solution of the problem. For scalar problems it is possible to estimate M by the initial condition as in [7] (M is proportional to the second derivative of the initial condition at smooth extrema), however it is more difficult to estimate M for the system case. If M is chosen too small, accuracy may degenerate at smooth extrema of the solution; however if M is chosen too large, oscillations will appear.

In [22] and in this paper we use the limiter described above to identify "troubled cells", namely, if one of the minmod functions gets enacted (returns other than the first argument), this cell is declared "troubled" and marked for further reconstructions. Since the HWENO reconstruction maintains the high order accuracy in the troubled cells, it is less crucial to choose an accurate M. We present in Section 3 numerical results obtained with different M's. Basically, if M is chosen too small, more good cells will be declared as troubled cells and will be subject to unnecessary HWENO reconstructions. This does increase the computational cost but does not degrade the order of accuracy in these cells.

For the troubled cells, we would like to reconstruct the polynomial solution while retaining its cell average. In other words, we will reconstruct the degrees of freedom, or the moments, $u_i^{(l)}$ for the troubled cell I_i for $l = 1, \ldots, k$ and retain only the cell average $u_i^{(0)}$.

For the third-order $k = 2$ case, we summarize the procedure to reconstruct the first and second moments $u_i^{(1)}$ and $u_i^{(2)}$ for a troubled cell I_i using HWENO:

Step 1. Reconstruction of the first moment $u_i^{(1)}$ by HWENO.

1. Given the small stencils $S_0 = \{I_{i-1}, I_i\}$, $S_1 = \{I_i, I_{i+1}\}$ and the bigger stencil $\mathscr{T} = \{S_0, S_1\}$, we construct Hermite quadratic reconstruction polynomials $p_0(x), p_1(x), p_2(x)$ and a fourth-degree reconstruction polynomial $q(x)$ such that:

$$\int_{I_{i+j}} p_0(x)\,\mathrm{d}x = u_{i+j}^{(0)} a_0, \quad j = -1, 0, \quad \int_{I_{i-1}} p_0(x) v_1^{(i-1)}(x)\,\mathrm{d}x = u_{i-1}^{(1)} a_1,$$

$$\int_{I_{i+j}} p_1(x)\,\mathrm{d}x = u_{i+j}^{(0)} a_0, \quad j = 0, 1, \quad \int_{I_{i+1}} p_1(x) v_1^{(i+1)}(x)\,\mathrm{d}x = u_{i+1}^{(1)} a_1,$$

$$\int_{I_{i+j}} p_2(x)\,\mathrm{d}x = u_{i+j}^{(0)} a_0, \quad j = -1, 0, 1,$$

$$\int_{I_{i+j}} q(x)\,\mathrm{d}x = u_{i+j}^{(0)} a_0, \quad j = -1, 0, 1, \quad \int_{I_{i+j}} q(x) v_1^{(i+j)}(x)\,\mathrm{d}x = u_{i+j}^{(1)} a_1, \quad j = -1, 1.$$

We now obtain:

$$\int_{I_i} p_0(x) v_1^{(i)}(x)\,\mathrm{d}x = a_1\Big(-2u_{i-1}^{(0)} + 2u_i^{(0)} - u_{i-1}^{(1)} \Big),$$

$$\int_{I_i} p_1(x) v_1^{(i)}(x)\,\mathrm{d}x = a_1\Big(-2u_i^{(0)} + 2u_{i+1}^{(0)} - u_{i+1}^{(1)} \Big),$$

$$\int_{I_i} p_2(x) v_1^{(i)}(x)\,\mathrm{d}x = a_1\Big(-u_{i-1}^{(0)} + u_{i+1}^{(0)} \Big) \Big/ 2,$$

$$\int_{I_i} q(x)v_1^{(i)}(x)\,\mathrm{d}x = a_l\left(\frac{15}{19}\left(u_{i-1}^{(0)} - u_{i+1}^{(0)}\right) - \frac{11}{38}\left(u_{i-1}^{(1)} + u_{i+1}^{(1)}\right)\right).$$

2. We find the combination coefficients, also called linear weights, denoted by γ_0, γ_1 and γ_2, satisfying:

$$\int_{I_i} q(x)v_1^{(i)}(x)\,\mathrm{d}x = \sum_{j=0}^{2}\gamma_j \int_{I_i} p_j(x)v_1^{(i)}(x)\,\mathrm{d}x,$$

which leads to

$$\gamma_0 = \frac{11}{38}, \quad \gamma_1 = \frac{11}{38}, \quad \gamma_2 = \frac{8}{19}.$$

3. We compute the smoothness indicator β_j by (2.7), and the nonlinear weights based on the smoothness indicators by (2.8). The first moment of the reconstructed polynomial is then given by

$$u_i^{(1)} = \frac{1}{a_1}\sum_{j=0}^{2}\omega_j \int_{I_i} p_j(x)v_1^{(i)}(x)\,\mathrm{d}x. \tag{3.5}$$

Step 2. Reconstruction of the second moment $u_i^{(2)}$ by HWENO. When the first moment $u_i^{(1)}$ is needed we use the reconstructed one from Step 1.

4. Given the small stencils $S_0 = \{I_{i-1}, I_i\}$, $S_1 = \{I_i, I_{i+1}\}$ and the bigger stencil $\mathscr{T} = \{S_0, S_1\}$, we construct Hermite cubic reconstruction polynomials $p_0(x), p_1(x), p_2(x)$ and a fifth-degree reconstruction polynomial $q(x)$ such that:

$$\int_{I_{i+j}} p_0(x)\,\mathrm{d}x = u_{i+j}^{(0)}a_0, \quad \int_{I_{i+j}} p_0(x)v_1^{(i+j)}(x)\,\mathrm{d}x = u_{i+j}^{(1)}a_1, \quad j = -1, 0,$$

$$\int_{I_{i+j}} p_1(x)\,\mathrm{d}x = u_{i+j}^{(0)}a_0, \quad \int_{I_{i+j}} p_1(x)v_1^{(i+j)}(x)\,\mathrm{d}x = u_{i+j}^{(1)}a_1, \quad j = 0, 1,$$

$$\int_{I_{i+j}} p_2(x)\,\mathrm{d}x = u_{i+j}^{(0)}a_0, \quad j = -1, 0, 1, \quad \int_{I_i} p_2(x)v_1^{(i)}\,\mathrm{d}x = u_i^{(1)}a_1,$$

$$\int_{I_{i+j}} q(x)\,\mathrm{d}x = u_{i+j}^{(0)}a_0, \quad \int_{I_{i+j}} q(x)v_1^{(i+j)}(x)\,\mathrm{d}x = u_{i+j}^{(1)}a_1, \quad j = -1, 0, 1,$$

which lead to

$$\int_{I_i} p_0(x)v_2^{(i)}(x)\,\mathrm{d}x = a_2\left(\frac{15}{4}u_{i-1}^{(0)} - \frac{15}{4}u_i^{(0)} + \frac{11}{8}u_{i-1}^{(1)} + \frac{19}{8}u_i^{(1)}\right),$$

$$\int_{I_i} p_1(x)v_2^{(i)}(x)\,\mathrm{d}x = a_2\left(-\frac{15}{4}u_i^{(0)} + \frac{15}{4}u_{i+1}^{(0)} - \frac{19}{8}u_i^{(1)} - \frac{11}{8}u_{i+1}^{(1)}\right),$$

$$\int_{I_i} p_2(x)v_2^{(i)}(x)\,\mathrm{d}x = a_2\left(\frac{1}{2}u_{i-1}^{(0)} - u_i^{(0)} + \frac{1}{2}u_{i+1}^{(0)}\right),$$

$$\int_{I_i} q(x)v_2^{(i)}\,\mathrm{d}x = a_2\left(\frac{73}{56}u_{i-1}^{(0)} - \frac{73}{28}u_i^{(0)} + \frac{73}{56}u_{i+1}^{(0)} + \frac{45}{112}u_{i-1}^{(1)} - \frac{45}{112}u_{i+1}^{(1)}\right).$$

5. We find the linear weights denoted by γ_0, γ_1 and γ_2 satisfying

$$\int_{I_i} q(x)v_2^{(i)}\,\mathrm{d}x(x) = \sum_{j=0}^{2}\gamma_j\int_{I_i} p_j(x)v_2^{(i)}(x)\,\mathrm{d}x,$$

which leads to

$$\gamma_0 = \frac{45}{154}, \quad \gamma_1 = \frac{45}{154}, \quad \gamma_2 = \frac{32}{77}.$$

6. We compute the smoothness indicator β_j by (2.10). The nonlinear weights are then computed based on the smoothness indicators using (2.8). The second moment of the reconstructed polynomial is then given by

$$u_i^{(2)} = \frac{1}{a_2}\sum_{j=0}^{2}\omega_j\int_{I_i} p_j(x)v_2^{(i)}(x)\,\mathrm{d}x. \qquad \square \tag{3.6}$$

4. Numerical results

In this section we present the results of our numerical experiments for the fifth-order HWENO schemes with the third-order TVD Runge–Kutta method (HWENO5-RK3) and the third-order DG method with HWENO limiter (DG3-HWENO5-RK3) developed in the previous sections, and compare them with the fifth-order finite volume WENO schemes in [26] and DG3 with TVB limiter [7]. A uniform mesh with N cells is used for all the test cases, the CFL number is taken as 0.8 for both HWENO5 and WENO5, and 0.18 for DG3-HWENO5-RK3 except for some accuracy tests where a suitably reduced time step is used to guarantee that spatial error dominates.

4.1. Accuracy tests

We first test the accuracy of the schemes on nonlinear scalar problems and nonlinear systems. In the accuracy tests the TVB constant M is taken as 0.01 (very close to a TVD limiter) for identifying the troubled cells in order to test the effect of the HWENO reconstruction for wrongly identified troubled cells in smooth regions.

Example 4.1. We solve the following nonlinear scalar Burgers equation

$$u_t + \left(\frac{u^2}{2}\right)_x = 0 \tag{4.1}$$

with the initial condition $u(x,0) = 0.5 + \sin(\pi x)$, and a 2-periodic boundary condition. When $t = 0.5/\pi$ the solution is still smooth, and the errors and numerical orders of accuracy by the HWENO5-RK3 scheme and by the WENO5-RK3 scheme [26] are shown in Table 1. We can see that both HWENO5-RK3 and WENO5-RK3 schemes achieve their designed order of accuracy, and HWENO5-RK3 produces smaller

Table 1
Burgers equation $u_t + (u^2/2)_x = 0$ with initial condition $u(x,0) = 0.5 + \sin(\pi x)$

N	HWENO5-RK3				WENO5-RK3			
	L_1 error	Order	L_∞ error	Order	L_1 error	Order	L_∞ error	Order
10	5.06E−03		1.79E−02		8.42E−03		2.67E−02	
20	4.93E−04	3.36	3.33E−03	2.43	1.04E−03	3.02	7.09E−03	1.91
40	3.65E−05	3.76	3.24E−04	3.36	8.86E−05	3.55	7.47E−04	3.25
80	1.61E−06	4.51	1.51E−05	4.43	4.17E−06	4.41	4.09E−05	4.19
160	6.25E−08	4.68	5.49E−07	4.78	1.67E−07	4.64	1.44E−06	4.82
320	1.86E−09	5.07	2.06E−08	4.74	5.14E−09	5.02	4.66E−08	4.95

HWENO5-RK3 and WENO5-RK3. $t = 0.5/\pi$. L_1 and L_∞ errors. Uniform meshes with N cells.

errors than WENO5-RK3 for the same mesh. Notice, however, that HWENO5-RK3 is almost twice as costly as WENO5-RK3 for the same mesh, as two reconstructions are involved for HWENO instead of just one for WENO. The results for DG3-HWENO5-RK3 and DG3-RK3 with no limiter are shown in Table 2. We can see that both schemes achieve their designed order of accuracy with comparable errors for the same mesh.

Example 4.2. We solve the following nonlinear system of Euler equations

$$u_t + f(u)_x = 0 \tag{4.2}$$

with

$$u = (\rho, \rho v, E)^{\mathrm{T}}, \quad f(u) = (\rho v, \rho v^2 + p, v(E+p))^{\mathrm{T}}.$$

Here ρ is the density, v is the velocity, E is the total energy, p is the pressure, which is related to the total energy by $E = p/\gamma - 1 + 1/2\rho v^2$ with $\gamma = 1.4$. The initial condition is set to be $\rho(x,0) = 1 + 0.2\sin(\pi x)$, $v(x,0) = 1$, $p(x,0) = 1$, with a 2-periodic boundary condition. The exact solution is $\rho(x,t) = 1 + 0.2\sin(\pi(x-t))$, $v(x,t) = 1$, $p(x,t) = 1$. We compute the solution up to $t = 2$. The errors and numerical orders of accuracy of the density ρ for the HWENO5-RK3 scheme are shown in Table 3, in comparison with the results of WENO5-RK3 in [26]. We can see that both schemes achieve their designed order of accuracy, and HWENO5-RK3 is more accurate than WENO5-RK3 on the same mesh. The results for DG3-HWENO5-RK3 and DG3-RK3 with no limiter are shown in Table 4. We can see that both schemes achieve their designed order of accuracy, however DG3-HWENO5-RK3 has larger errors for the same mesh.

Table 2
Burgers equation $u_t + (u^2/2)_x = 0$ with initial condition $u(x,0) = 0.5 + \sin(\pi x)$

N	DG with HWENO limiter				DG with no limiter			
	L_1 error	Order	L_∞ error	Order	L_1 error	Order	L_∞ error	Order
10	1.41E−02		8.09E−02		3.35E−03		2.21E−02	
20	1.12E−03	3.66	7.09E−03	3.51	4.00E−04	3.07	3.59E−03	2.62
40	7.99E−05	3.81	5.78E−04	3.62	5.11E−05	2.97	5.78E−04	2.64
80	8.34E−06	3.26	8.26E−05	2.81	6.46E−06	2.98	8.26E−05	2.81
160	9.97E−07	3.06	1.14E−05	2.86	8.14E−07	2.99	1.14E−05	2.86
320	1.22E−07	3.03	1.50E−06	2.92	1.02E−07	2.99	1.50E−06	2.92

DG3-HWENO5-RK3 and DG3-RK3 with no limiters. $t = 0.5/\pi$. L_1 and L_∞ errors. Uniform meshes with N cells.

Table 3
Euler equations. $\rho(x,0) = 1 + 0.2\sin(\pi x)$, $v(x,0) = 1$, $p(x,0) = 1$

N	HWENO5-RK3				WENO5-RK3			
	L_1 error	Order	L_∞ error	Order	L_1 error	Order	L_∞ error	Order
10	3.33E − 03		5.10E − 03		6.63E − 03		5.92E − 03	
20	1.28E − 04	4.70	2.43E − 04	4.39	3.04E − 04	4.45	2.91E − 04	4.35
40	3.82E − 06	5.07	7.34E − 06	5.05	9.08E − 06	5.06	9.19E − 06	4.99
80	1.17E − 07	5.02	2.30E − 07	5.00	2.80E − 07	5.02	2.95E − 07	4.96
160	3.62E − 09	5.02	6.54E − 09	5.14	8.72E − 09	5.00	8.67E − 09	5.09
320	1.08E − 10	5.06	1.85E − 10	5.14	2.71E − 10	5.01	2.45E − 10	5.15

HWENO5-RK3 and WENO5-RK3 using N equally spaced cells. $t = 2$. L_1 and L_∞ errors of density ρ.

Table 4
Euler equations. $\rho(x,0) = 1 + 0.2\sin(\pi x)$, $v(x,0) = 1$, $p(x,0) = 1$

N	DG with HWENO limiter				DG with no limiter			
	L_1 error	Order	L_∞ error	Order	L_1 error	Order	L_∞ error	Order
10	2.79E − 03		4.51E − 03		1.41E − 05		2.17E − 05	
20	1.05E − 04	4.73	4.46E − 04	3.34	8.14E − 07	4.11	1.29E − 06	4.08
40	2.31E − 05	2.18	4.51E − 05	3.31	7.06E − 08	3.53	1.11E − 07	3.54
80	3.27E − 06	2.82	5.36E − 06	3.07	7.84E − 09	3.17	1.23E − 08	3.17
160	4.21E − 07	2.96	6.98E − 07	2.94	9.49E − 10	3.05	1.49E − 09	3.05
320	5.30E − 08	2.99	9.87E − 08	2.82	1.18E − 10	3.01	1.85E − 10	3.01

DG3-HWENO5-RK3 and DG3-RK3 with no limiter, using N equally spaced cells. $t = 2$. L_1 and L_∞ errors of density ρ.

4.2. Test cases with shocks

Example 4.3. We solve the same nonlinear Burgers equation (4.1) as in Example 4.1 with the same initial condition $u(x,0) = 0.5 + \sin(\pi x)$, except that we now plot the results at $t = 1.5/\pi$ when a shock has already appeared in the solution. In Fig. 1, the solutions of HWENO5-RK3 (left) and DG3-HWENO5-RK3 (right) with $N = 80$ cells are shown. The solid line is the exact solution. We can see that both schemes give non-oscillatory shock transitions for this problem.

Example 4.4. We solve the nonlinear non-convex scalar Buckley–Leverett problem

$$u_t + \left(\frac{4u^2}{4u^2 + (1-u)^2}\right)_x = 0 \tag{4.3}$$

with the initial data $u = 1$ when $-\frac{1}{2} \leqslant x \leqslant 0$ and $u = 0$ elsewhere. The solution is computed up to $t = 0.4$. The exact solution is a shock-rarefaction-contact discontinuity mixture. We remark that some high order schemes may fail to converge to the correct entropy solution for this problem. In Fig. 2, the solutions of HWENO5-RK3 (left) and DG3-HWENO5-RK3 (right) with $N = 80$ cells are shown. The solid line is the exact solution. We can see that both schemes give good resolutions to the correct entropy solution for this problem.

Example 4.5. We solve the Euler equations (4.2) with a Riemann initial condition for the Lax Problem

$$(\rho, v, p) = (0.445, 0.698, 3.528) \quad \text{for } x \leqslant 0, \quad (\rho, v, p) = (0.5, 0, 0.571) \quad \text{for } x > 0.$$

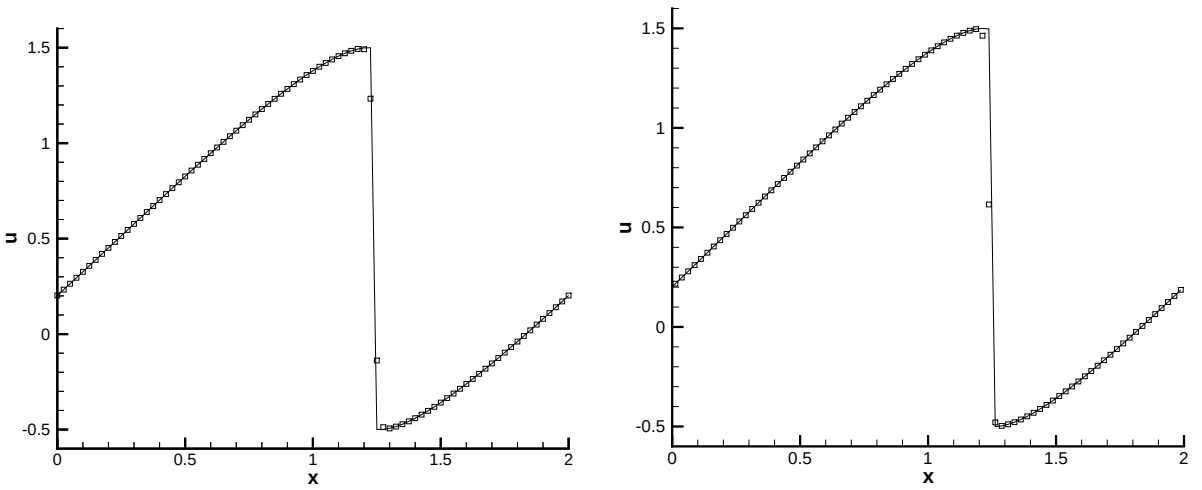

Fig. 1. Burgers equation. $u(x,0) = 0.5 + \sin(\pi x)$. $t = 1.5/\pi$. HWENO5-RK3 (left) and DG3-HWENO5-RK3 (right) with $N = 80$ cells. Solid line: exact solution; squares: computed solution.

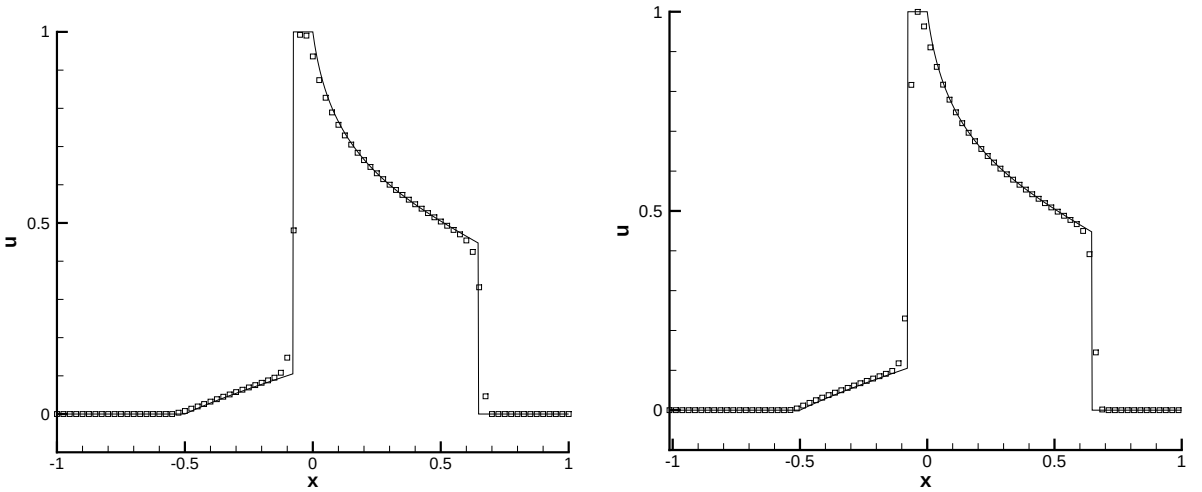

Fig. 2. The Buckley–Leverett problem. $t = 0.4$. HWENO5-RK3 (left) and DG3-HWENO5-RK3 (right) with $N = 80$ cells. Solid line: exact solution; squares: computed solution.

The computed density ρ is plotted at $t = 1.3$ against the exact solution. In Fig. 3 we plot the solution with $N = 200$ cells by HWENO5-RK3 and WENO5-RK3, and in Fig. 4 we show the results of the DG3-HWENO5-RK3 scheme with different TVB constants M in identifying the troubled cells, with the time history of cells being identified as troubled cells shown in Fig. 5. We can see that both HWENO5-RK3 and DG3-HWENO5-RK3 give equally good non-oscillatory shock transitions for this problem, and the parameter M has a significant effect in determining how many cells are identified as troubled cells. This indicates a need for better strategy for identifying troubled cells, which we plan to investigate in the future.

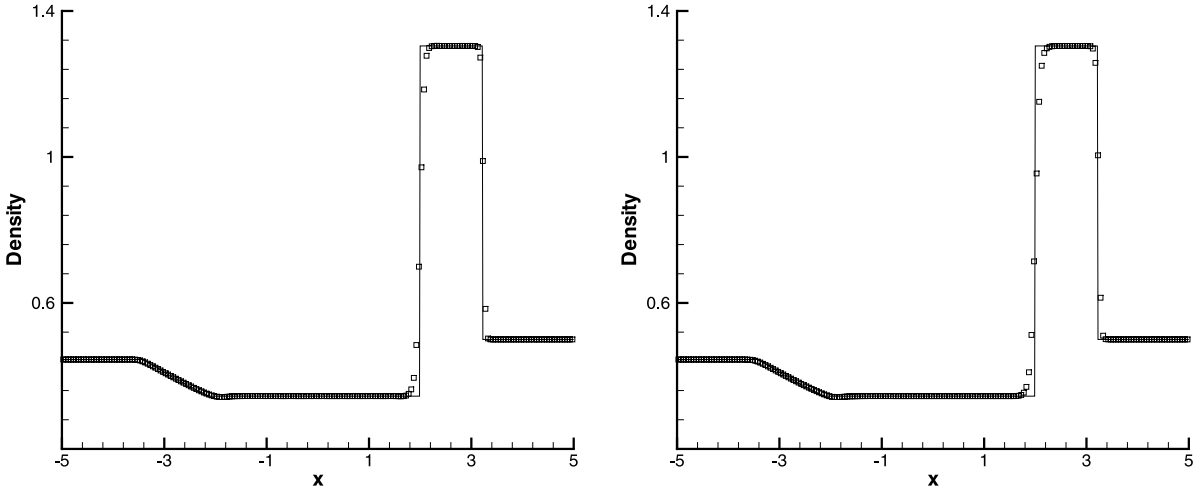

Fig. 3. The Lax problem. $t = 1.3$. HWENO5-RK3 (left) and WENO5-RK3 (right), $N = 200$ cells. Density ρ. Solid line: exact solution; squares: computed solution.

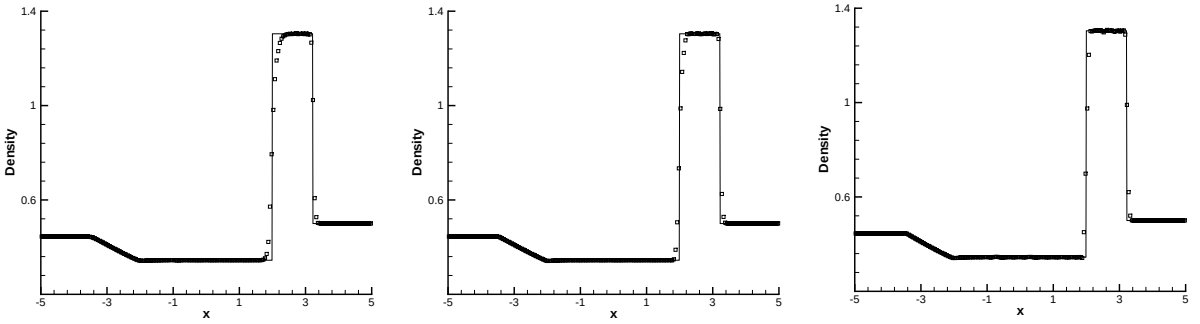

Fig. 4. Lax problem by DG3-HWENO5-RK3 with 200 cells, with the TVB constant $M = 0.01$ (left), $M = 10.0$ (middle) and $M = 50$ (right). $t = 1.3$. Density ρ. Squares are the computed solution and solid lines are the exact solution.

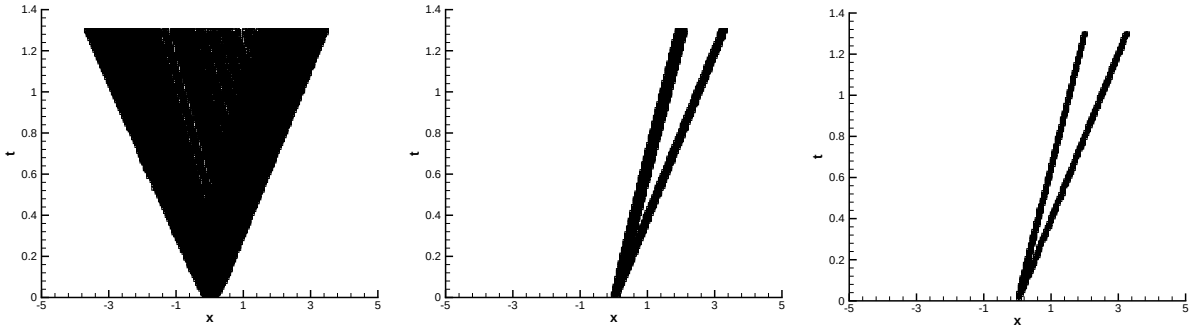

Fig. 5. Lax problem by DG3-HWENO5-RK3 with 200 cells, with the TVB constant $M = 0.01$ (left), $M = 10.0$ (middle) and $M = 50$ (right). $t = 1.3$. Time history of troubled cells. Squares are the troubled cells where the HWENO limiters are used.

Example 4.6. The previous examples contain only shocks and simple smooth region solutions (almost piecewise linear), for which shock resolution is the main concern and usually a good second-order non-oscillatory scheme would give satisfactory results. There is little advantage in using higher order schemes for such cases. We have been using them in the numerical experiments mainly to demonstrate the non-oscillatory properties of the high order schemes. A higher order scheme would show its advantage when the solution contains both shocks and complex smooth region structures. A typical example for this is the problem of shock interaction with entropy waves [28]. We solve the Euler equations (4.2) with a moving Mach = 3 shock interacting with sine waves in density, i.e. initially

$$(\rho, v, p) = (3.857143, 2.629369, 10.333333) \quad \text{for } x < -4,$$

$$(\rho, v, p) = (1 + \varepsilon \sin 5x, 0, 1) \quad \text{for } x \geqslant -4.$$

Here we take $\varepsilon = 0.2$. The computed density ρ is plotted at $t = 1.8$ against the reference solution, which is a converged solution computed by the fifth-order finite difference WENO scheme [17] with 2000 grid points.

In Fig. 6 we show the results of the HWENO5-RK3 and WENO5-RK3 schemes with $N = 300$ cells, and in Figs. 7 and 8 we show the results of the DG3-HWENO5-RK3 scheme with $N = 200$ cells and the time history of trouble cells where HWENO limiters are used. We can see that the $N = 200$ results for DG3-HWENO5-RK3 with a higher value of M are comparable with the HWENO5-RK3 or WENO5-RK3 results with $N = 300$ cells.

Example 4.7. We consider the interaction of blast waves of Euler equation (4.2) with the initial condition

$$(\rho, v, p) = (1, 0, 1000) \quad \text{for } 0 \leqslant x < 0.1,$$

$$(\rho, v, p) = (1, 0, 0.01) \quad \text{for } 0.1 \leqslant x < 0.9,$$

$$(\rho, v, p) = (1, 0, 100) \quad \text{for } 0.9 \leqslant x.$$

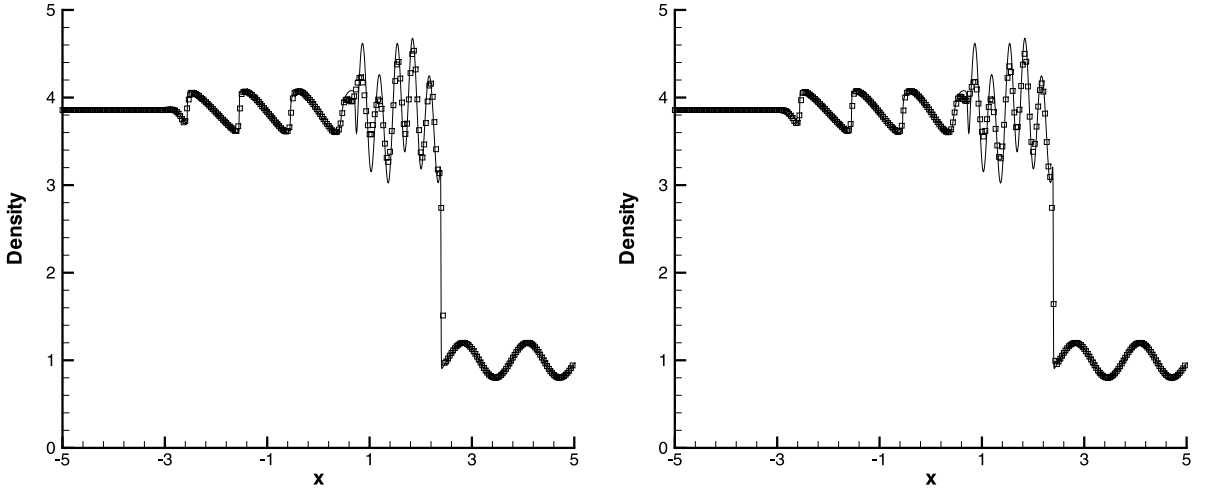

Fig. 6. The shock density wave interaction problem. $t = 1.8$. HWENO5-RK3 (left) and WENO5-RK3 (right) with $N = 300$ cells. Density ρ. Solid line: "Exact solution"; squares: computed solution.

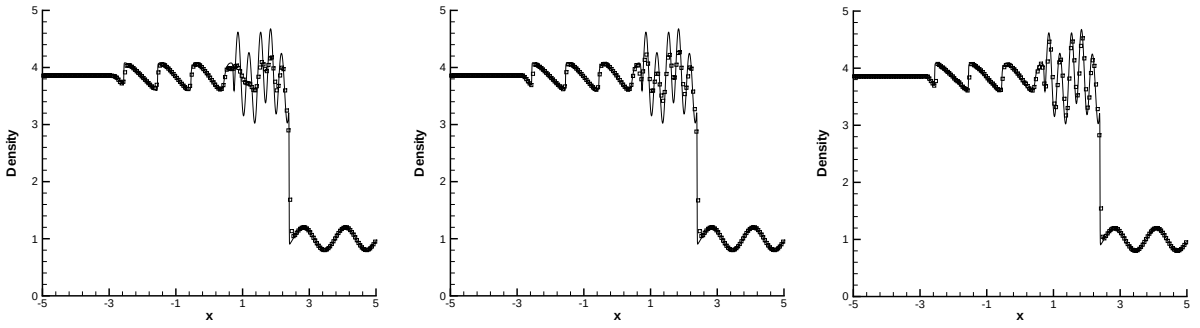

Fig. 7. The shock density wave interaction problem by DG3-HWENO5-RK3 with 200 cells, $t = 1.8$, with TVB constant $M = 0.01$ (left), $M = 50.0$ (middle) and $M = 300$ (right). Density ρ. Solid line: "Exact solution"; squares: computed solution.

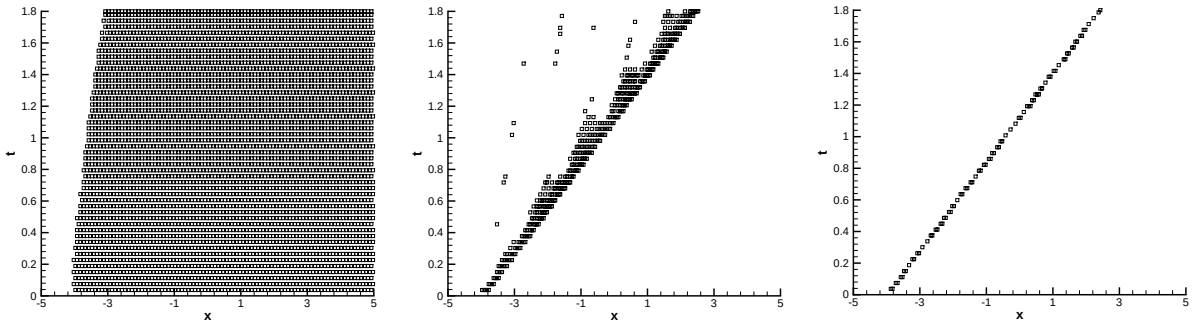

Fig. 8. The shock density wave interaction problem by DG3-HWENO5-RK3 with 200 cells, $t = 1.8$, with TVB constant $M = 0.01$ (left), $M = 50.0$ (middle) and $M = 300$ (right). Time history of troubled cells. Squares are the troubled cells where the HWENO limiters are used.

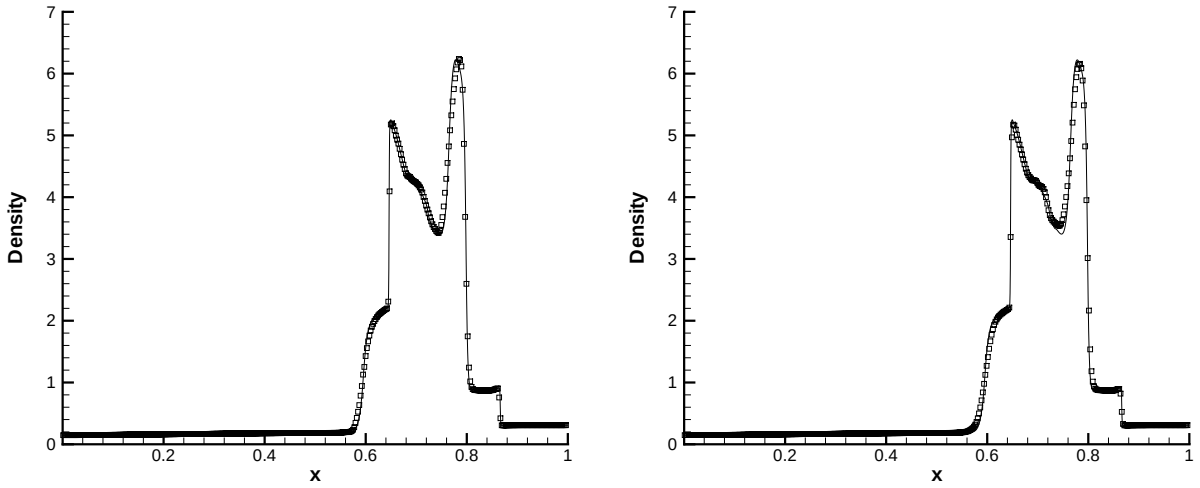

Fig. 9. The interaction of blast waves problem by HWENO5-RK3 (left) and WENO5-RK3 (right) with 400 cells, $t = 0.038$. Density ρ. Squares are the computed solution and solid lines are the "exact" reference solution.

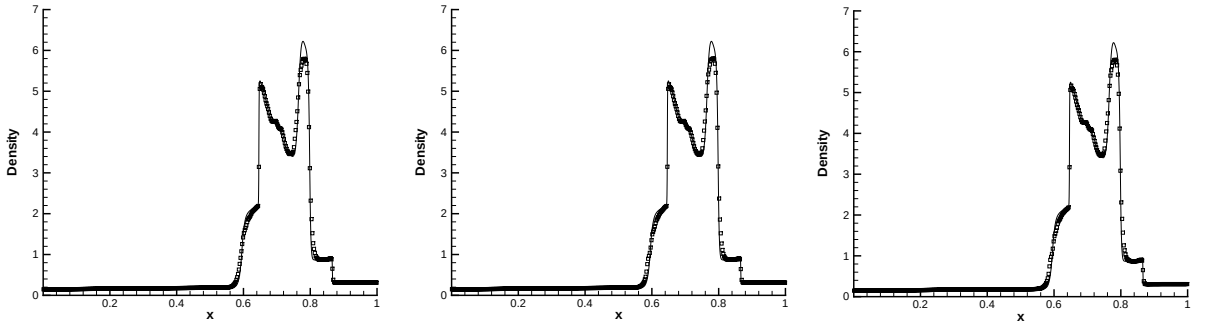

Fig. 10. The interaction of blast waves problem by DG3-HWENO5-RK3 with 400 cells, $t = 0.038$, with the TVB constant $M = 0.01$ (left), $M = 50.0$ (middle) and $M = 300$ (right). Density ρ. Squares are the computed solution and solid lines are the "exact" reference solution.

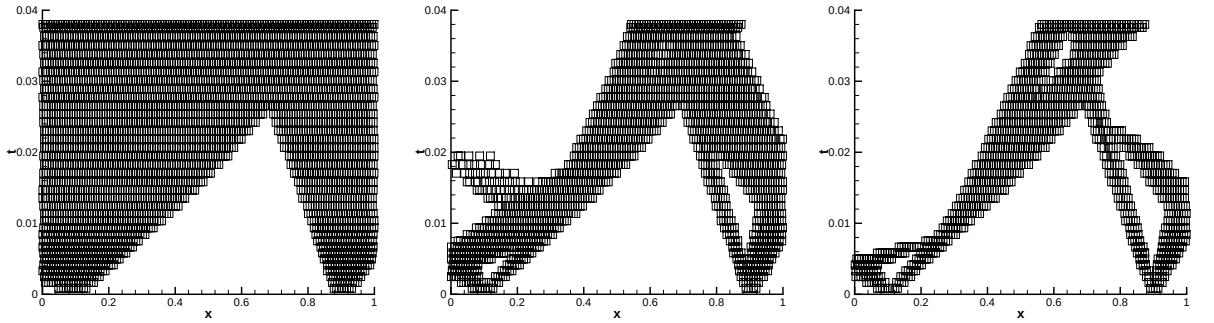

Fig. 11. The interaction of blast waves problem by DG3-HWENO5-RK3 with 400 cells, $t = 0.038$, with the TVB constant $M = 0.01$ (left), $M = 50.0$ (middle) and $M = 300$ (right). Time history of troubled cells. Squares are the troubled cells where the HWENO limiters are used.

A reflecting boundary condition is applied to both ends. See [15,30]. The computed density ρ is plotted at $t = 0.038$ against the reference "exact" solution, which is a converged solution computed by the fifth-order finite difference WENO scheme [17] with 2000 grid points.

In Fig. 9 we show the results of the HWENO5-RK3 and WENO5-RK3 schemes with $N = 400$ cells, and in Figs. 10 and 11 we show the results of the DG3-HWENO5-RK3 scheme with $N = 400$ cells as well as the time history of troubled cells where HWENO limiters are used.

5. Concluding remarks

In this paper, we have constructed a new class the fifth-order WENO schemes, which we termed HWENO (Hermite WENO) schemes, for solving nonlinear hyperbolic conservation law systems. The construction of HWENO schemes is based on a finite volume formulation, Hermite interpolation, and Runge–Kutta methods. The idea of reconstruction for HWENO comes from the WENO schemes. In the HWENO schemes, both the function and its first derivative are evolved in time and used in the reconstruction, in contrast to the regular WENO schemes where only the function value is evolved in time and used in the reconstruction. Comparing with the regular WENO schemes, one major advantage of HWENO schemes is their relatively compact stencil. This makes HWENO schemes more suitable for limiters in the

Runge–Kutta discontinuous Galerkin methods, the application of this is also presented in this paper. Extensive numerical experiments are performed to verify the accuracy and non-oscillatory shock resolution of both the HWENO scheme and the RKDG method with HWENO limiters. Only the 1D case is considered in this paper. While the methodology can be generalized in principle to multi dimensions, more work is needed to carry out the detailed design and this is left for future research.

References

[1] D.S. Balsara, C.-W. Shu, Monotonicity preserving weighted essentially non-oscillatory schemes with increasingly high order of accuracy, Journal of Computational Physics 160 (2000) 405–452.
[2] R. Biswas, K.D. Devine, J. Flaherty, Parallel, adaptive finite element methods for conservation laws, Applied Numerical Mathematics 14 (1994) 255–283.
[3] F. Bouchut, C. Bourdarias, B. Perthame, A MUSCL method satisfying all the numerical entropy inequalities, Mathematics of Computation 65 (1996) 1439–1461.
[4] A. Burbeau, P. Sagaut, C.H. Bruneau, A problem-independent limiter for high-order Runge–Kutta discontinuous Galerkin methods, Journal of Computational Physics 169 (2001) 111–150.
[5] B. Cockburn, S. Hou, C.-W. Shu, The Runge–Kutta local projection discontinuous Galerkin finite element method for conservation laws IV: the multidimensional case, Mathematics of Computation 54 (1990) 545–581.
[6] B. Cockburn, S.-Y. Lin, C.-W. Shu, TVB Runge–Kutta local projection discontinuous Galerkin finite element method for conservation laws III: one-dimensional systems, Journal of Computational Physics 84 (1989) 90–113.
[7] B. Cockburn, C.-W. Shu, TVB Runge–Kutta local projection discontinuous Galerkin finite element method for conservation laws II: general framework, Mathematics of Computation 52 (1989) 411–435.
[8] B. Cockburn, C.-W. Shu, The Runge–Kutta local projection P1-discontinuous Galerkin finite element method for scalar conservation laws, Mathematical Modelling and Numerical Analysis (M^2AN) 25 (1991) 337–361.
[9] B. Cockburn, C.-W. Shu, The Runge–Kutta discontinuous Galerkin method for conservation laws V: multidimensional systems, Journal of Computational Physics 141 (1998) 199–224.
[10] B. Cockburn, C.-W. Shu, Runge–Kutta discontinuous Galerkin method for convection-dominated problems, Journal of Scientific Computing 16 (2001) 173–261.
[11] M.G. Crandall, A. Majda, Monotone difference approximations for scalar conservation laws, Mathematics of Computation 34 (1980) 1–21.
[12] R.L. Dougherty, A.S. Edelman, J.M. Hyman, Nonnegativity-, monotonicity-, or convexity-preserving cubic quintic Hermite interpolation, Mathematics of Computation 52 (1989) 471–494.
[13] O. Friedrichs, Weighted essentially non-oscillatory schemes for the interpolation of mean values on unstructured grids, Journal of Computational Physics 144 (1998) 194–212.
[14] A. Harten, High resolution schemes for hyperbolic conservation laws, Journal of Computational Physics 49 (1983) 357–393.
[15] A. Harten, B. Engquist, S. Osher, S. Chakravathy, Uniformly high order accurate essentially non-oscillatory schemes, III, Journal of Computational Physics 71 (1987) 231–303.
[16] C. Hu, C.-W. Shu, Weighted essentially non-oscillatory schemes on triangular meshes, Journal of Computational Physics 150 (1999) 97–127.
[17] G. Jiang, C.-W. Shu, Efficient implementation of weighted ENO schemes, Journal of Computational Physics 126 (1996) 202–228.
[18] D. Levy, G. Puppo, G. Russo, Central WENO schemes for hyperbolic systems of conservation laws, Mathematical Modelling and Numerical Analysis 33 (1999) 547–571.
[19] X. Liu, S. Osher, T. Chan, Weighted essentially non-oscillatory schemes, Journal of Computational Physics 115 (1994) 200–212.
[20] T. Nakamura, R. Tanaka, T. Yabe, K. Takizawa, Exactly conservative semi-Lagrangian scheme for multi-dimensional hyperbolic equations with directional splitting technique, Journal of Computational Physics 174 (2001) 171–207.
[21] J. Qiu, C.-W. Shu, On the construction, comparison, local characteristic decomposition for high order central WENO schemes, Journal of Computational Physics 183 (2002) 187–209.
[22] J. Qiu, C.-W. Shu, Runge–Kutta discontinuous Galerkin method using WENO limiters, submitted to SIAM Journal on Scientific Computing.
[23] W.H. Reed, T.R. Hill, Triangular mesh methods for neutron transport equation, Tech. Report LA-UR-73-479, Los Alamos Scientific Laboratory, 1973.
[24] J. Shi, C. Hu, C.-W. Shu, A technique of treating negative weights in WENO schemes, Journal of Computational Physics 175 (2002) 108–127.
[25] C.-W. Shu, TVB uniformly high-order schemes for conservation laws, Mathematics of Computation 49 (1987) 105–121.

[26] B. Cockburn, C. Johnson, C.-W. Shu, E. Tadmor, Essentially non-oscillatory and weighted essentially non-oscillatory schemes for hyperbolic conservation laws, in: A. Quarteroni (Ed.), Advanced Numerical Approximation of Nonlinear Hyperbolic Equations, Lecture Notes in Mathematics, vol. 1697, Springer, Berlin, 1998, pp. 325–432.
[27] C.-W. Shu, S. Osher, Efficient implementation of essentially non-oscillatory shock-capturing schemes, Journal of Computational Physics 77 (1988) 439–471.
[28] C.-W. Shu, S. Osher, Efficient implementation of essentially non-oscillatory shock capturing schemes II, Journal of Computational Physics 83 (1989) 32–78.
[29] H. Takewaki, A. Nishiguchi, T. Yabe, Cubic interpolated pseudoparticle method (CIP) for solving hyperbolic type equations, Journal of Computational Physics 61 (1985) 261–268.
[30] P. Woodward, P. Colella, The numerical simulation of two-dimensional fluid flow with strong shocks, Journal of Computational Physics 54 (1984) 115–173.